Icarus **155**, 285–298 (2002)
doi:10.1006/icar.2001.6749, available online at http://www.idealibrary.com on IDEAL®

Statistical Analysis of the Links among Lunar Mare Soil Mineralogy, Chemistry, and Reflectance Spectra

Carlé M. Pieters

Department of Geological Sciences Brown University, Providence, Rhode Island 02912
E-mail: Carle_Pieters@brown.edu

D. G. Stankevich and Yu. G. Shkuratov

Astronomical Observatory of Kharkov State University, 35 Sumskaya St., Kharkov 310022, Ukraine

and

L. A. Taylor

Planetary Geosciences Institute, University of Tennessee, Knoxville, Tennessee 37996

Received February 28, 2001; revised July 31, 2001

A principal goal of the Lunar Soil Characterization Consortium (LSCC) is to evaluate tools that might be successfully used in remote compositional analysis of the lunar surface. Mathematical methods are extremely valuable to assess whether variations exist in a statistically significant manner, independent of their interpretation. The bounds of widely used correlation of visible to near-infrared spectral parameters with composition are first defined and evaluated. We then evaluate direct (or indirect) links between the combined spectral properties of lunar mare soils and their compositional properties (elemental abundance and mineralogy) through a statistical analysis of the variance across each measurement using principal component analysis (PCA). We first separately analyze LSCC elemental abundance, mineralogy, and spectroscopy data (0.35 to 2.5 μm) using PCA to capture the variance of each system with a relatively small number of independent variables. With this compact set of independent variables for each type of data, we derive functions to link composition and spectroscopy. For these mare soils, one of the best empirical predictive capability is that for FeO. This is not surprising since the effect of ferrous iron on optical properties is well documented. Although Al_2O_3 has no direct effect on optical properties, its strong anticorrelation with FeO also produces a relatively high predictive capability from spectra. Similarly, a high accuracy in predicting the abundance of pyroxene is observed and should be expected since iron-bearing pyroxene is one of the most optically active components of lunar soil. The accuracy for predicting either TiO_2 or ilmenite, on the other hand, is disappointing. High- and low-Ti soils are readily distinguished, but these statistics suggest that making subclass distinctions based on spectral predictions of TiO_2 would be risky. © 2002 Elsevier Science (USA)

1. INTRODUCTION

Visible and near-infrared reflectance spectra of the Moon depend on the physical characteristics and composition (chemical and mineralogical) of the lunar regolith. In this spectral region, principal chromophores in lunar materials are the transition elements iron and titanium, which have unfilled *d* orbitals. Electronic transitions within (or between) Fe and Ti ions produce diagnostic features in ultraviolet, visible, and near-infrared wavelengths (Burns 1993). Pyroxene, olivine, and ilmenite are the main Fe- and Ti-bearing minerals in lunar surface materials, although glasses and native iron are also present. Plagioclase feldspar (a Ca–Al silicate) is the most abundant mineral of the lunar crust, but it accommodates little iron in its structure (<0.3%).

There have been several attempts to study the relationships between optical and chemical characteristics and to use these relations to predict the elemental abundance of the chromophores Fe and Ti. (e.g., Adams 1974, Charette *et al.* 1974, Pieters 1978, Johnson and Singer 1991, Jaumann 1991, Lucey *et al.* 1995, 1998, Shkuratov *et al.* 1999a). A challenge in such efforts is also to accommodate the influence of alteration in the space environment and the effects of soil maturity on optical properties. For returned soils, such soil maturity effects, or cumulative exposure to the space environment, are often estimated with the ratio I_s/FeO (e.g., Morris 1976, 1978), which is the amount of single-domain nanophase Fe^0 in the soil normalized to the FeO content, where I_s is measured by ferromagnetic resonance techniques. This nanophase reduced iron (npFe^0) is formed during

0019-1035/02 $35.00

sputtering and micrometeorite impact vaporization and accumulates on the surface of grains, as well as within the impact-formed agglutinitic glass. The character and abundance of the $npFe^0$ dominates the optical properties of space weathering (Keller *et al*. 2000, Pieters *et al*. 2000a, Taylor *et al*. 2000, 2001a,b, Noble *et al*. 2001). Accumulation of $npFe^0$ lowers the albedo, weakens absorption bands, and affects the continuum in a manner dependent on the total abundance (Pieters *et al*. 2000a, Noble *et al*. 2001). Most approaches acknowledge the presence of these space weathering effects on lunar samples and derive empirical relations between compositional and optical data to incorporate both compositional and alteration variations.

Such empirical links between composition and optical properties are not necessarily limited to variations in Fe and Ti. Correlations naturally exist between some rock-forming elements and between some elements and minerals. Empirical relations thus can be derived between the optical properties and the abundance of nonchromophore elements, which do not themselves directly affect the optical properties. For instance, empirical relations have been used to predict the abundance of aluminum due to its strong anticorrelation with iron (Fischer and Pieters 1995) and ^3He due to its tendency to accumulate in ilmenite (Johnson *et al*. 1999, Shkuratov *et al*. 1999b).

The purpose of this paper is to test various statistical methods that can be used to find significant relationships between characteristics of laboratory reflectance spectra of lunar regolith samples and chemical parameters of the samples (such as Fe and Ti concentrations and the ratio I_s/FeO). Although the use and interpretation of any relation between optical parameters and composition must be based on an understanding of the natural physics of the system, statistical methods are valuable to assess whether variations are really significant. In the following sections, we analyze and compare various linear correlations and regressions with principal component analysis (PCA). We first discuss the character of the compositional and spectral data and then details of the various approaches. We summarize the results that can be obtained from this limited set of data as well as the potential return from a more comprehensive data set.

2. DATA DESCRIPTION

2.1. Lunar Soil Characterization Consortium

The data included in this analysis are the coordinated detailed measurements for a suite of lunar mare soils produced by the Lunar Soil Characterization Consortium (LSCC) (Taylor *et al*. 2000, 2001a,b). These include nine lunar mare regolith samples from the Apollo 11, 12, 15, and 17 missions, selected to be representative of various basalt compositions with different degrees of soil "maturity" (alteration in the space environment). Coordinated compositional and spectroscopic measurements were obtained for four subsamples of each of the nine soils. These subsamples have controlled particle size: <45, <10, 10–20, and 20–45 μm. The <45-μm sample is considered to represent the bulk soil since it has been amply demonstrated that the optical properties of bulk soils are dominated by the smaller size fractions (Pieters *et al*. 1993a, Fischer 1995).

TABLE I
Example of Chemical Composition Measured for LSCC: 15071 Soil Separates

	Size range (sample)			
	<45 (,173)	20–45 (,176)	10–20 (,180)	<10 (,184)
SiO_2	45.9 (4)	45.8 (3)	45.7 (3)	46.9 (2)
TiO_2	1.81 (15)	2.33 (7)	1.88 (24)	1.57 (8)
Al_2O_3	13.1 (3)	12.4 (2)	12.9 (3)	17.1 (1)
Cr_2O_3	0.41 (6)	0.43 (4)	0.53 (8)	0.40 (3)
MgO	11.3 (2)	11.4 (1)	11.0 (3)	9.85 (9)
CaO	10.3 (1)	9.81 (1)	10.2 (3)	11.8 (1)
MnO	0.19 (2)	0.21 (3)	0.22 (4)	0.15 (2)
FeO	14.9 (2)	15.6 (3)	15.4 (4)	9.59 (17)
NiO	<0.03	<0.03	<0.03	<0.03
Na_2O	0.37 (3)	0.36 (2)	0.39 (2)	0.48 (2)
K_2O	0.13 (2)	0.14 (1)	0.18 (2)	0.22 (2)
P_2O_5	0.18 (9)	0.15 (8)	0.19 (7)	0.09 (8)
SO_2	0.12 (7)	0.10 (6)	0.10 (8)	0.14 (5)
Totals	98.71	98.73	98.69	98.30
I_s/FeO	71	49	~80	159

To minimize physical effects of sample preparation, all size separates were prepared with ultrapure deionized water (Noble *et al*. 2001). Bidirectional spectra were obtained for all samples using the RELAB spectrometer to include the spectral range 0.3–2.6 μm (Pieters *et al*. 2000b). Detailed chemical analyses were obtained for all subsamples and mineralogical data were obtained for the size separates 20–45, 10–20, and <10 μm (Taylor *et al*. 2000, 2001a,b). An example of the chemical and mineralogical data for one soil (15071) is provided in Tables I and II. Spectra for this sample are shown in Fig. 1.

2.2. Spectral Information

Since the diagnostic features of minerals in the visible and near-infrared occur as light is transmitted through the medium, most quantitative analyses are performed in some form of a logarithmic scale to accommodate the natural requirements for absorption coefficients (Beer's Law). There are several methods to transform a reflectance measurement (a linear measurement of intensity) into the equivalent of an absorption coefficient, ranging from simple reformatting into a logarithmic scale (e.g., Sunshine *et al*. 1990) to using scattering models which incorporate radiative transfer (Hapke 1981, 1993) and physical models (Hiroi and Pieters 1992, 1994). We use the model by Shkuratov *et al*. (1999c), which is specifically designed to accommodate the properties of lunar and planetary regolith.

The Shkuratov *et al*. model describes light scattering from particulate surfaces and incorporates geometrical optics with the optical constants n and k, the real and imaginary parts of the refractive index. Radiation propagating between points is

TABLE II
Example of Mineral Abundance Measured for LSCC: 15071 Soil Separates

	Size range (sample)			
	20–45 μm (,178)		10–20 μm (,182)	
# Particles	1799		2730	
Pixel count	308379		124092	
	Mode (%)	Normalized	Mode (%)	Normalized
plagiodase	17.71	18.27	18.71	19.43
ilmenite	1.63	1.69	1.70	1.77
olivine	3.79	3.91	2.66	2.77
VG: Ti-glass	0.40	0.42	0.50	0.52
VG: Green	3.64	3.75	3.47	3.61
MgCpx	6.76	6.98	5.36	5.56
FeCpx	1.55	1.60	1.30	1.38
Pigeonite	9.95	10.27	7.45	7.64
Opx	3.12	3.22	1.98	2.13
Total PX	21.38	22.07	16.08	16.71
Aggl.	46.17	47.63	45.42	49.17
CrSp	0.11	0.12	0.60	0.62
SiO_2	0.83	0.86	1.61	1.67
K-glass	1.25	1.29	1.31	1.36
Unclassified	3.07		3.71	
FeS			0.07	0.07

characterized by the absorption coefficient $\tau = 4\pi\kappa l/\lambda$, where l is the average length of light propagation in a particle between internal reflections. The model is formally one dimensional, but it takes into account key properties of the three-dimensional case. In particular, it contains a porosity coefficient μ, which is the volume fraction of the medium (regolith) filled with particles. An important characteristic of the model is its reversibility; i.e., the function $\kappa(\lambda)$ can be found if the bidirectional spectral albedo $A(\lambda)$ is known and estimates for the parameters n, l, and μ are available. The principal formulation of this model (Shkuratov *et al.* 1999c) is

$$\kappa(\lambda) = -\frac{\lambda}{4\pi l}\ln\left[\frac{b}{a} + \sqrt{\left(\frac{b}{a}\right)^2 - \frac{c}{a}}\right], \qquad (1)$$

where a, b, and c incorporate information about Fresnel reflections (internal and external) from the particulate medium. These three terms (a, b, c) are multi component terms and are derived from n, A, μ and Fresnel coefficients (see Shkuratov *et al.* 1999c). Note that in this formulation, $\kappa(\lambda)$ represents the extinction coefficient, the imaginary part of the complex index of refraction.

Using formula (1), the extinction coefficient $\kappa(\lambda)$ was derived for each spectrum assuming the real part of the index of refraction $n = 1.5$ and porosity $\mu = 0.5$. For each particle size separate, an estimate of l, the average length of light propagation between interfaces, was first estimated from the mean grain size. For particle size separates <10, 10–20, 20–45, and bulk <45 μm, l was first estimated to be 5, 15, 32, and 22 μm, respectively. The extinction coefficient $\kappa(\lambda)$ should be independent of variations in particle size. However, the initial estimates of $\kappa(\lambda)$ for soil 15071, using the above values for l, exhibit unreasonably large spectrum-to-spectrum variations. (shown in Fig. 2). Although small variations with wavelength are expected due to compositional trends that have been documented as a function of particle size (Taylor *et al.* 2000, 2001a,b), extinction coefficients from the *same* soil should be similar in parts of the spectrum that are not affected by mineral variations. The large offsets among $\kappa(\lambda)$ values for different size fractions observed in Fig. 2 is an indication that one or more of the original assumptions about path length are not correct.

A more realistic estimation for l should account for the fact that the grain size of individual elements within a soil particle involved in the interaction with light is normally much smaller

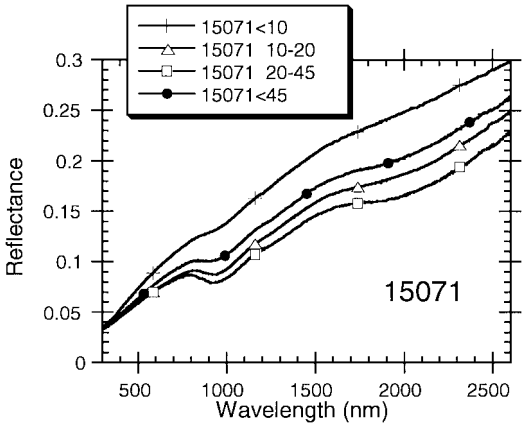

FIG. 1. Bidirectional reflectance spectra for separates of mare soil 15071.

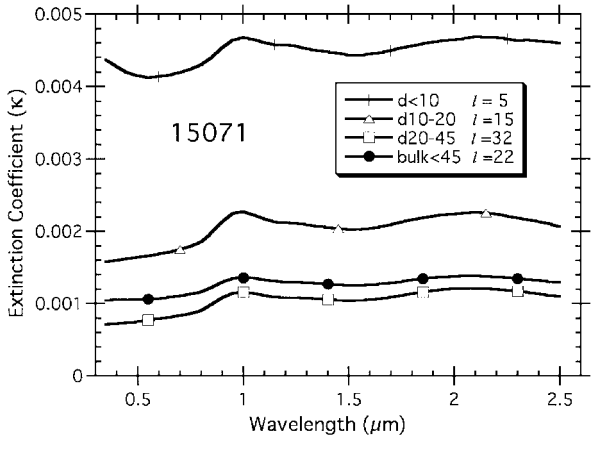

FIG. 2. Preliminary calculation of extinction coefficients $\kappa(\lambda)$ for the particle size separates of lunar sample 15071. The average length of light propagation (l) was assumed to be the mean particle size.

TABLE III
Average Distance (in μm) of Light Propagation (l) in Grains of Mare Soil Size Separates

Sample	<10 μm	10–20 μm	20–45 μm	<45 μm bulk
10084	8.4	10	11.6	9.7
12001	7.4	10	12.0	9.9
12030	6.3	10	10.9	8.8
15041	6.3	10	11.2	8.9
15071	7.3	10	11.0	9.1
70181	7.7	10	12.2	10.5
71061	6.5	10	12.5	8.6
71501	8.4	10	10.9	10.0
79221	7.6	10	11.5	9.2

than the particle size itself, because most particles are multicomponent. For most fractions of a given soil (e.g., <45 μm), the average grain size should be roughly comparable for all soil size separates until mechanical processes break them into smaller grains to avoid errors resulting from inaccurate estimates of the average length of light propagation, l was estimated to be equal to 10 μm for the 10–20 μm sample, and values of l for all other separates were then derived. To accomplish this, $\kappa(\lambda)$ spectra for all separates of a given soil are assumed to be equal at 1.5 μm, a wavelength that is free of known absorptions. We then derive empirical values of l for each of the separates. The results for all mare soils are summarized in Table III. The consistency of values of l for all size separates except the smallest (as expected) provides confidence in these revised estimates. An example of the resulting $\kappa(\lambda)$ spectra for mare soil separates is shown in Fig. 3. Values of $\kappa(\lambda)$ derived in this manner are used in the PCA analyses of Section 4.

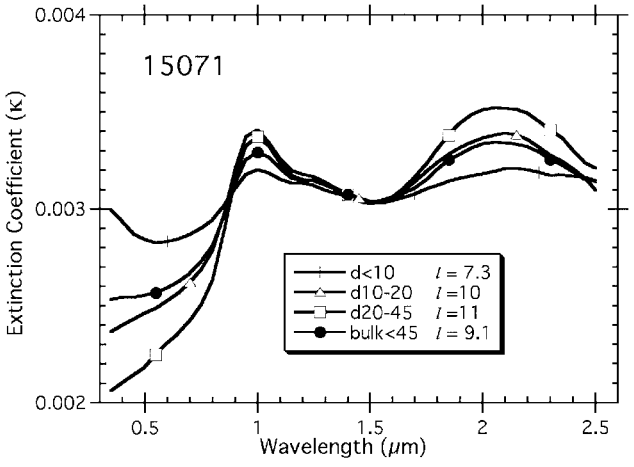

FIG. 3. Calculated extinction coefficients $\kappa(\lambda)$ for the particle size separates of lunar sample 15071. The extinction coefficient was assumed to be the same at 1.5 μm for all size separates of the same soil. Because the grain size is much smaller than the particle size, the average length of light propagation (l) in a grain was assumed to be equal to 10 μm for the 10–20 μm sample and was derived for other size separates.

3. CORRELATION APPROACH

Parameters that are systematically related to each other in a linear manner are easily recognized by a well-defined trend in a plot of one variable against another. Standard mathematical correlation coefficients express a simple statistical measure of any relationship between two variables. High correlations between parameters usually result from systematic relations in the natural system—rules governing how minerals form, the composition of specific minerals, and the regular mineral composition of different rock types. Similarly, optical absorptions that result from specific minerals or components of minerals should result in explicit correlation between optical properties and composition. Conversely, if a high correlation is found between two measured parameters, it is often assumed there is some direct or indirect relation between them, and a measure of one might be used to predict the other. Correlations between various types of data collected for the LSCC mare soils are presented below. Some results are expected, with sound geologic explanations. Others have less obvious causes, if any.

3.1. Correlation between Compositions

Presented in Tables IV, V and VI are correlation coefficients showing relationships between chemical parameters, mineral parameters, and chemistry vs mineral parameters respectively for this suite of mare soils. Correlations greater than 0.70 (absolute) are highlighted in boldface (excluding duplicates). Recall that the chemical data consist of four size separates (bulk <45, 20–45, 10–20, and <10 μm) for each of nine soils, whereas the mineral data were only obtained for individual size separates but not the bulk <45 μm (see Taylor *et al*. 2001b).

In spite of the limited range of the samples (all are basaltic soils), some well-known chemical correlations (e.g., see Heiken *et al*. 1991, Chap. 7) are easily identified in Table IV: the almost perfect anticorrelation between FeO and Al_2O_3 and between TiO_2 and SiO_2. It is also reassuring that, in spite of their low abundance, a strong correlation is evident between the relatively volatile components K_2O and P_2O_5.

Correlations among mineral abundances (Table V) are less strong. Nevertheless, abundance of agglutinates is anticorrelated with everything except plagioclase and "other" (combined minor components). This is largely because agglutinates grow at the expense of mineral components. Plagioclase is an exception to this anticorrelation since communition enriches plagioclase in the finer fractions, which is also the principal feedstock that melts to form agglutinitic glass (e.g., Taylor *et al*. 2000, 2001b).

Chemistry–mineral correlations (Table VI) are controlled by several competing relationships. Mineral chemistry clearly dominates the strong correlation between ilmenite abundance and TiO_2. On the other hand, regolith processes control the correlation of agglutinate abundance with Al_2O_3 and anticorrelation with FeO, as plagioclase is incorporated into agglutinitic melt.

None of these compositional correlations are particularly surprising. They nevertheless provide a rational backdrop for

TABLE IV
Chemical Correlations (×100) among LSCC Mare Soil Samples

	SiO_2	TiO_2	Al_2O_3	Cr_2O_3	MgO	CaO	MnO	FeO	Na_2O	K_2O	P_2O_5	SO_2	I_s/FeO
SiO_2	—	−97.95	25.18	1.00	12.16	−12.88	−42.56	−28.2	38.56	84.97	88.9	−48.13	20.26
TiO_2	**−97.95**	—	−28.42	−7.31	−24.29	14.14	43.37	30.81	−33.53	−76.65	−82.17	47.76	−23.73
Al_2O_3	25.18	−28.42	—	−51.36	−52.6	81.25	−85.21	−98.72	72.0	26.91	21.87	20.77	86.76
Cr_2O_3	1.00	−7.31	−51.36	—	60.68	−73.84	43.59	55.37	−27.83	1.01	−5.45	4.56	−59.65
MgO	12.16	−24.20	−52.60	60.68	—	−75.23	41.76	49.99	−63.34	−22.71	−14.15	−33.88	−37.62
CaO	−12.88	14.14	**81.25**	**−73.84**	**−75.23**	—	−65.37	−82.58	55.02	−2.72	−4.278	28.44	80.89
MnO	−42.56	43.37	**−85.21**	43.59	41.76	−65.37	—	87.13	−77.17	−44.75	−35.83	−12.09	−72.84
FeO	−28.20	30.81	**−98.72**	55.37	49.99	**−82.58**	**87.13**	—	−70.91	−28.03	−23.26	−17.68	−91.56
Na_2O	38.56	−33.5	**72.40**	−27.83	−63.34	55.02	**−77.17**	**−70.91**	—	67.36	48.41	28.83	49.34
K_2O	**84.97**	**−76.65**	26.91	1.01	−22.71	−2.72	−44.75	−28.03	67.36	—	90.35	−17.7	11.47
P_2O_5	88.9	**−82.17**	21.87	−5.45	−14.15	−4.28	−35.83	−23.26	48.41	**90.35**	—	−40.31	13.35
SO_2	−48.13	47.76	20.77	4.56	−33.88	28.44	−12.09	−17.68	28.83	−17.7	−40.31	—	3.004
I_s/FeO	20.26	−23.73	**86.76**	−59.65	−37.62	**80.89**	**−72.84**	**−91.56**	49.34	11.47	13.35	3.004	—

Note. Correlations greater than 0.70 are bold.

correlations between composition and optical properties discussed in Section 5.

3.2. Correlation between Composition and Spectral Ratios

One of the earliest and most common methods for measuring the color of an object is to construct a simple ratio derived from measurement at one wavelength divided by measurement at another wavelength. Empirical correlations of such color ratios with composition have been widely used, largely because color ratios are relatively simple to obtain and a good correlation justifies their use. We discuss two such correlations between color ratios and composition as examples here.

TiO_2. Before modern computers permeated approaches to data analysis, correlations between parameters were painstakingly analyzed on a case-by-case basis with data for one variable plotted against another. For lunar science, one of the earliest relationships recognized was one between the abundance of TiO_2 in lunar mare soils and the slope of the visible continuum (Charette *et al*. 1974). Relatively "blue" basalts are Ti-rich, and relatively "red" basalts are Ti-poor, with a ratio of ultraviolet (UV) radiation (400 nm) to visible (VIS) radiation (560 nm) being the color ratio used. It was later thought that extending the VIS range to longer wavelengths (e.g., ∼750 nm) might improve the measurement accuracy (e.g., Johnson and Singer 1991). More advanced methods of optimization were used by Blewett *et al*. (1997), Lucey *et al*. (1998, 2000), and by Shkuratov *et al*. (1999a) to map the estimated variation of TiO_2 across the Moon. Various causes of this empirical relation between UV/VIS color and TiO_2 have been proposed (Pieters 1993, Pieters *et al*. 1993b, Lucey *et al*. 2000). Although complete consensus on the origin of this relationship has not been forthcoming, the UV/VIS color ratio has been one of the most widely used spectral parameters in lunar exploration. To a first order, it has worked well for mare soils (e.g., see recent Hiesinger *et al*. 2000).

Since spectral information is available for all LSCC data from 0.3 to 2.5 μm, we have broadened the correlation analysis to

TABLE V
Mineral–Mineral Correlations (×100)

	Ilm	Plag	Px	OI	AG	VG	Other
Ilm	—	13.98	−23.67	37.6	−45.36	73.80	−85.76
Plag	13.98	—	−30.77	−7.54	3.50	−1.08	−15.7
Px	−23.67	−30.77	—	39.31	−64.75	−24.89	41.17
OI	37.6	−7.54	39.31	—	−75.74	54.06	−40.66
AG	−45.36	3.50	−64.75	**−75.74**	—	−51.25	25.31
VG	**73.80**	−1.08	−24.89	54.06	−51.25	—	−79.82
Other	**−85.76**	−15.7	41.17	−40.66	25.31	**−79.82**	—

Note. Ilm, ilmenite; Plag, plagioclase; Px, pyroxene (all types); Ol, olivine; AG, agglutinitic glass; VG, volcanic glass (all types); Other, combined other minor components.

TABLE VI
Chemistry–Mineral Correlations (×100)

	Ilm	Plag	Px	OI	AG	VG	Other
SiO_2	**−94.10**	−21.47	28.57	−31.10	40.35	**−74.14**	**85.25**
TiO_2	**93.32**	16.57	−21.89	24.62	−40.83	67.20	**−79.91**
Al_2O_3	−26.25	28.92	**−76.19**	−62.49	**83.80**	−23.39	4.69
Cr_2O_3	11.76	5.95	35.84	64.84	−60.16	27.70	1.64
MgO	−9.77	−14.87	45.22	64.47	−45.04	15.39	−0.95
CaO	5.00	24.82	**−78.87**	**−74.05**	**73.72**	−10.64	−12.22
MnO	35.62	5.16	58.88	55.89	**−79.15**	28.26	−17.73
FeO	28.52	−23.36	**73.83**	66.58	**−86.95**	28.06	−6.48
Na_2O	−29.17	−0.62	−47.28	−53.30	61.41	−22.42	21.01
K_2O	**−73.71**	−23.42	19.55	−34.76	37.42	−62.67	**72.18**
P_2O_5	**−83.60**	−23.4	27.02	−42.62	39.09	**−73.93**	**85.05**
SO_2	51.59	9.19	−41.15	14.71	−4.40	49.18	−54.24
I_s/FeO	−23.31	14.78	−68.47	**−70.44**	**86.21**	−31.30	3.64

Note. Ilm, ilmenite; Plag, plagioclase; Px, pyroxene (all types); Ol, olivine; AG, agglutinitic glass; VG, volcanic glass (all types); Other, combined other minor components.

include all color ratios at 50-nm intervals over this wider spectral range. Results for TiO_2 are shown in matrix form in Figs. 4a and 4b. Each point in the figure represents the color ratio for the two wavelengths indicated by the axes. The intensity at each point is the correlation coefficient of that color ratio with TiO_2 abundance as measured for the lunar mare soils in our study. Density shading used to designate the magnitude of the coefficient is comparable for direct and anticorrelations. For Fig. 4a, the input data are color ratios derived directly from the bidirectional reflectance measurements. For Fig. 4b,. the input data are ratios of approximate extinction coefficients (color indices) derived from the reflectance data as described above.

The high correlation of UV/VIS with TiO_2 abundance that stimulated the empirical use of this parameter for predictions of TiO_2 is recognized in the lower left corner of Figs. 4a and 4b. There are several important aspects of this relation that have not been recognized before. First, UV/VIS correlations in reflectance data for mare soils (Fig. 4a) are good (0.60 to 0.70) but not excellent. They are best for the wavelength range used by Charette *et al*. (1974), i.e., 400/560 nm, but begin to drop

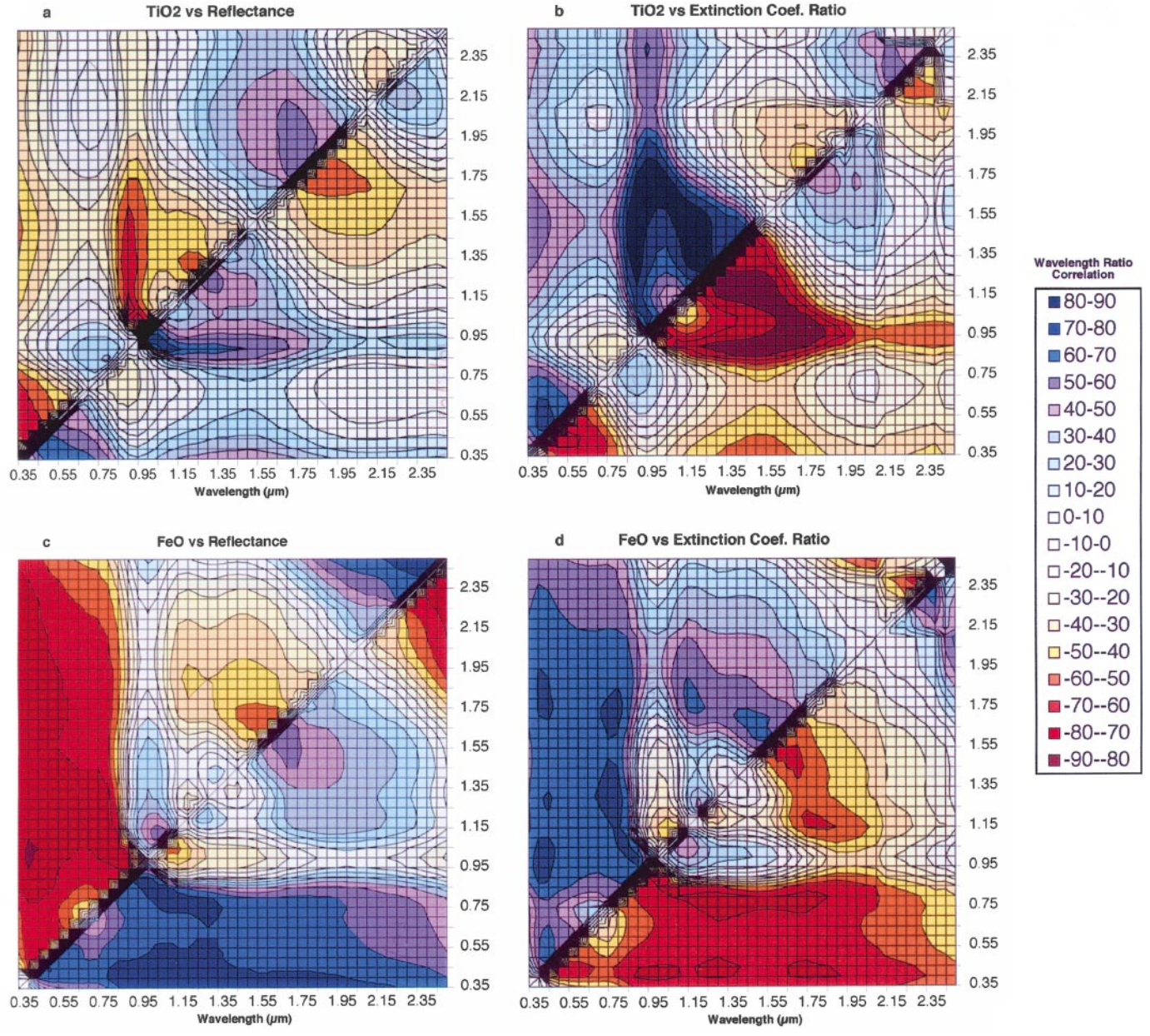

FIG. 4. Correlation of spectral ratios with chemistry for LSCC mare soils. Each point in the matrix represents the spectral ratio of values indicated on the axes. The intensity at each point is the correlation coefficient of values of that spectral ratio to the chemical parameter indicated: (a) reflectance ratios correlated with TiO_2, (b) extinction coefficient ratios correlated with TiO_2, (c) reflectance ratios correlated with FeO, (d) extinction coefficient ratios correlated with FeO.

when the wavelength range is extended much further. For example, the correlation is only 0.54 for wavelengths comparable to those measured by Clementine (400/750 nm). In the extinction coefficient ratios (Fig. 4b), the narrow range of UV/VIS color ratios with high correlation to TiO_2 becomes obvious and the correlation improves.

Note that a second rather extensive curved zone of high correlation between color ratios and TiO_2 exists at longer wavelengths. These correlations are even higher than that observed in the UV, but in the same sense (flatter spectra correlated with higher TiO_2). The zone outlines ratios that measure the steepness of the spectrum on the long-wavelength side of principal ferrous absorptions near 950 and 1200 nm.

The effects of Ti-bearing species on spectral contrast (Pieters 1993, Pieters *et al*. 1993b) is likely to play a role in these correlations, especially those at longer wavelengths. It is also important to note that our Apollo 17 soils all contain abundant volcanic glass (Taylor *et al*. 2000, 2001a), and the optical properties of ilmenite are directly detectable in some samples at shorter wavelengths (Pieters *et al*. 2000b). The modest correlations of UV/VIS ratios for mare soils could well be a combination of low spectral contrast and the short wavelength portion of the broad ilmenite band seen in Apollo 17 volcanic black beads.

FeO. Since highly diagnostic absorption bands due to ferrous iron are known to exist in lunar spectra near 1 and 2 μm (e.g., Burns 1993, Pieters 1993), one would expect to find some correlation of ratios with FeO abundance near those wavelengths. The results for FeO, shown in Figs. 4c and 4d, are very instructive and help illuminate the difficulty of using a simple parameter to capture such a relation. The broad region of moderate to high correlation along the bottom and left of the figures indicates that any ratio of a value between 400 and 800 nm to that at a longer wavelength in the near-infrared provides a correlation with FeO abundance of at least 0.50 (except for a small zone close to 700 nm). In other words, spectra with a "flatter" continuum in such a short-wavelength/long-wavelength ratio are correlated with FeO abundance, and "steeper" spectra are more Al-rich. This may, however, simply be an artifact of the overall character of the input soil data. For each soil, small size fractions have steeper slopes over this range than larger size fractions (due largely to the concentration of the weathering product nanophase metallic iron in the fine fraction) and the fine fraction also has a higher concentration of Al-rich agglutinitic glass. Thus, the zone of high correlation between color and FeO reflects this systematic relation of composition and weathering products with particle size among these mare soil samples.

Correlation with the widely used 750/950 nm ratio from Clementine analyses falls between 0.60 and 0.70, but it is not the highest correlation over the range of silicon detectors (400 to 1000 nm). The highest correlation (near 0.80) is in fact for 1000/400 nm. This is most clearly seen in the extinction coefficient data (Fig. 4d), where the highest correlation occurs for ratios between 400 nm and 1000, 1300, and 1800 nm, near where ferrous absorption bands occur in mare soils (e.g., Noble *et al*. 2000). The sensitivity of spectral parameters that link FeO composition to ratios between 400 nm data and ferrous band centers may be related to the very regular manner in which lunar spectra of all size fractions of natural soils approach the same value near 400 nm (Pieters *et al*. 1993a).

4. PCA APPROACH

The correlation discussion in Section 3 demonstrates relations that can be recognized with simple two-parameter comparisons. Let us now turn to more sophisticated approaches that utilize a multivariant system. For most groups of measurements, individual variables are not fully independent from each other. As shown in the above compositional measurements, some elements correlate or anticorrelate with others due to well-defined principles of mineral formation. Similarly, neighboring measurements at different wavelengths of a spectrum are highly correlated. The first issue then is to develop a framework that recognizes the principal independent variations within a given data set.

4.1. General Principles

Principal component analysis is a powerful analytical tool to find internal correlations within a set of data and to develop a linear representation of these statistical data requiring a minimal number of independent values. It is a method to capture the variance of a system with a relatively small number of independent variables. We summarize aspects of this approach that are relevant to compositional assessment and prediction. The technique as applied to planetary surfaces is reviewed in Johnson *et al*. (1985) and Jaumann (1991).

Consider a number N of objects, each of them characterized by a set of K parameters, with $K < N$. In other words, each object could be represented as a point in a K-dimensional space of the parameters. These parameters cannot be all totally independent of each other. In other words, points representing the objects do not fill the K-dimensional space uniformly but form some subspace with a smaller number of dimensions. To find the optimal dimensions of this subspace we need to build a covariance matrix C containing the initial parameter set,

$$C_{j,k} = \sum_{i=1}^{N} p_{i,j}\, p_{i,k}, \tag{2}$$

where $1 \le i \le N$; i is the index of object, $1 \le k \le K$; and k is the index of parameter, and then we solve for the eigenvalues.

From matrix algebra, the eigenvalues β_q of any matrix C with nonzero determinant can be expressed as

$$C \cdot \varphi_q = \beta_q \varphi_q, \tag{3}$$

where φ_q is the group of eigenfunctions (also known as eigenvectors) of the given matrix. The number of eigenvalues Q

equals the matrix rank, i.e., the number of linearly independent rows or columns in the matrix. All eigenvalues β_q are positive since the initial covariance matrix is symmetrical. Sorting the eigenfunctions in decreasing order of eigenvalues we obtain a new linear orthogonal representation of the initial set of parameters. The parameters for any object would now be represented as a series,

$$p_{i,k} = \sum_{q=1}^{Q} a_{i,q}\varphi_{q,k}, \tag{4}$$

where $a_{i,q}$ are the so-called loading coefficients. These coefficients ($a_{i,q}$) are related to the initial parameter set $p_{i,k}$ by a similar equation:

$$a_{i,q} = \sum_{k=1}^{K} p_{i,k}\varphi_{q,k}, \qquad 1 \le q \le Q. \tag{5}$$

In this representation, each object now needs Q (instead of K) new coefficients $a_{i,q}$ to fully characterize all initial parameters $p_{i,k}$. If there are linear dependencies among the initial set of parameters, we have $Q < K$, and the new formulation is a much more compact representation of the initial data. Strictly speaking, experimentally measured data contain random errors or noise which destroy any linear dependence among parameters, and we have $Q = N > K$. A positive feature of PCA analysis, however, is that the loading coefficients $a_{i,q}$ decrease in magnitude rapidly with the eigenfunction number. Thus, we can normally restrict the series by a few terms. For experimental data sets, three or four eigenfunctions and respective loading coefficients are normally sufficient to describe the inherent variance of the data (see examples in Section 4.3).

PCA identifies the main axes of variance in K-dimensional space for a data cloud consisting of points representing the objects. The first eigenfunction (φ_1) corresponds to the direction of the longest axis of variance and the first eigenvalue (β_1) for a given object is an indication of the object's variability along this axis. The second eigenfunction shows the second (orthogonal) axis of variation and so on. The variability of objects described by the higher order axes (typically of order 5 or more) is much smaller and can often be ignored. Subtle but important variations that are more difficult to interpret, however, may still be present in the higher orders (e.g., Jaumann 1991).

4.2. PCA Applied to Chemistry and Mineralogy

Using the PCA technique described in Section 4.1, we derive a system of eigenfunctions for the chemical and mineralogical constituents of the suite of lunar mare soil samples studied by the LSCC. The objective is to capture the principal components that account for compositional variations of these samples. Components that vary directly or inversely are not independent, thus allowing the total variation to be captured in a few eigenfunctions. The result are shown graphically in Fig. 5. The eigenvalues, an indication of the amount of variance captured by each eigenfunction, decrease dramatically from the first to fourth eigenfunction.

For soil chemistry, there is much interdependence among the chemical parameters. This nonindependence is clearly seen in the symmetry observed comparing the first two eigenfunctions in Fig. 5a. The first eigenfunction captures the strong anticorrelation of SiO_2 and TiO_2 (Table IV). The first and second eigenfunctions capture the anticorrelation of FeO and Al_2O_3. In this

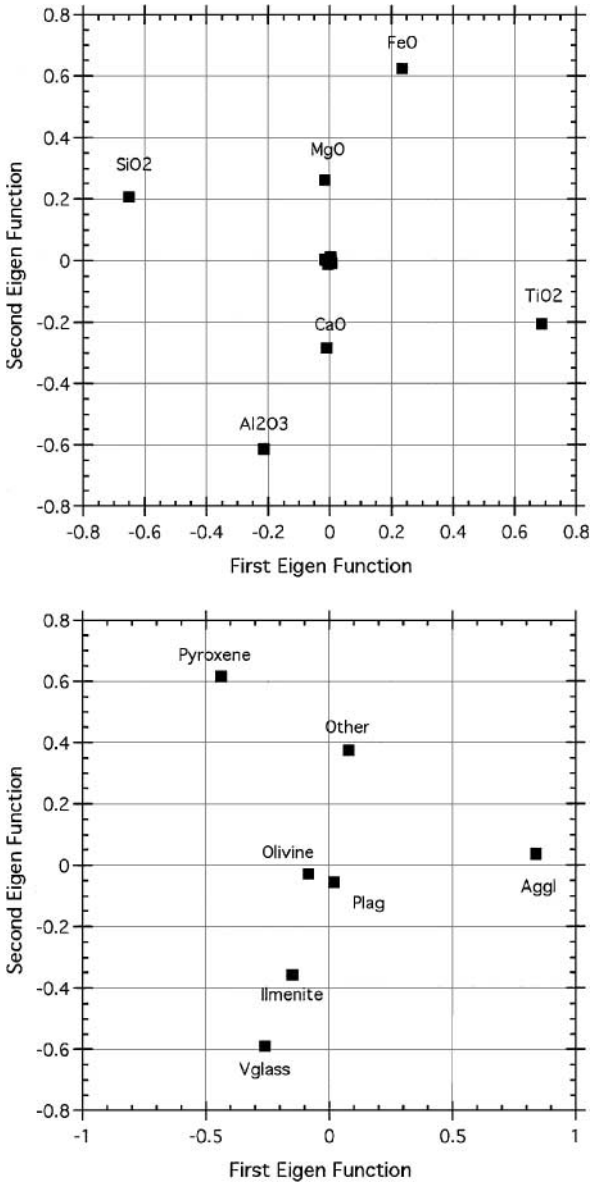

FIG. 5. Comparison of values for the first two eigenfunctions of mare soil compositional data. Eigenvalues (β_q) indicate that most of the variance is captured by the first two eigenfunctions. (Top) Comparison of values for chemical data. The center cluster includes the minor elements measured that contribute less than 1% (see Table I). The first four eigenvalues (β_q) are 439, 197, 20.4, and 2.4. (Bottom) Comparison of values for mineralogy data. The first four eigenvalues (β_q) are 2420, 1340, 129, and 98.

suite of mare soils, it is seen that K_2O, P_2O_3, Cr_2O_3 Na_2O, SO_2, and MnO contribute little to systematic variations among samples.

The eigenfunctions for soil mineralogy (Fig. 5b) describe less coupling of minerals than those derived for soil chemistry. The anticorrelation of agglutinates with everything except plagioclase and "other" is captured by the first eigenfunction.

Although the results of this PCA analysis for mare soil chemistry and mineralogy do not provide any big surprises, they do provide insight into the statistical framework of principal component analysis.

4.3. PCA Applied to Spectral Data

In preparation for PCA analysis of spectral properties, the spectra were first re-sampled in 0.05-μm steps over the wavelength range 0.35–2.5 μm. This re-sampling simplifies the eigenfunction analysis. Because the LSCC soil spectra are smooth and accurate in the wavelength range considered, little information was lost as a consequence of this re-sampling.

In reality, the real number of independent values in a spectrum is much smaller than the number of "independent" measurements at different wavelengths of the spectrum. Strong correlations exist between neighboring points within a spectrum. PCA provides a means to reduce the number of variables needed to describe an individual spectrum from a given group of N spectra. Each spectrum $\kappa_i(\lambda)$ can be described by an expanding series of eigenfunctions,

$$\kappa_i(\lambda) = \bar{\kappa}(\lambda) + \sum_{q=1}^{Q} a_{i,q}\varphi_q(\lambda), \tag{6}$$

where $\varphi_q(\lambda)$ are eigenfunctions, a_{iq} are expanding coefficients for the ith spectrum, and $\bar{\kappa}(\lambda)$ is the average spectrum of the whole group of spectra. Formally, the number of eigenfunctions Q is equal to the rank of the covariance matrix, but the expanding coefficients decrease rapidly with the number q. This allows any spectrum to be described by three or four coefficients a_q with high accuracy. Since principal component analysis determines nonrandom variations of spectra (real spectral features) that contribute to eigenfunctions (with small numbers q), it provides stability to the results with respect to random noise.

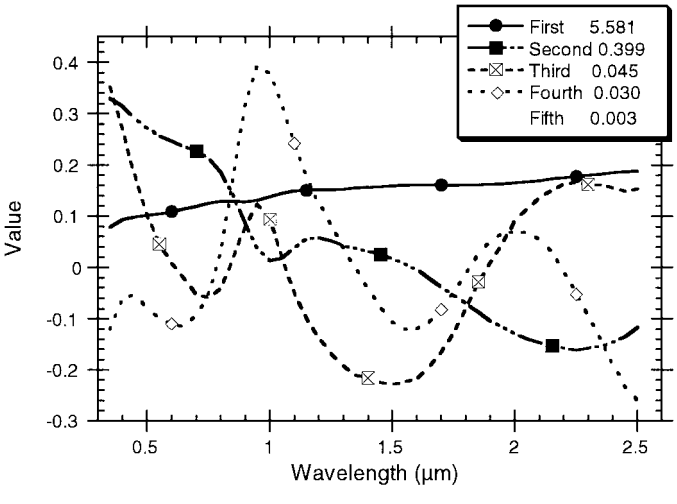

FIG. 6. Eigenfunctions for $\kappa(\lambda)$ spectra of LSCC lunar mare soils. Eigenvalues (β_q) for each are shown in the legend.

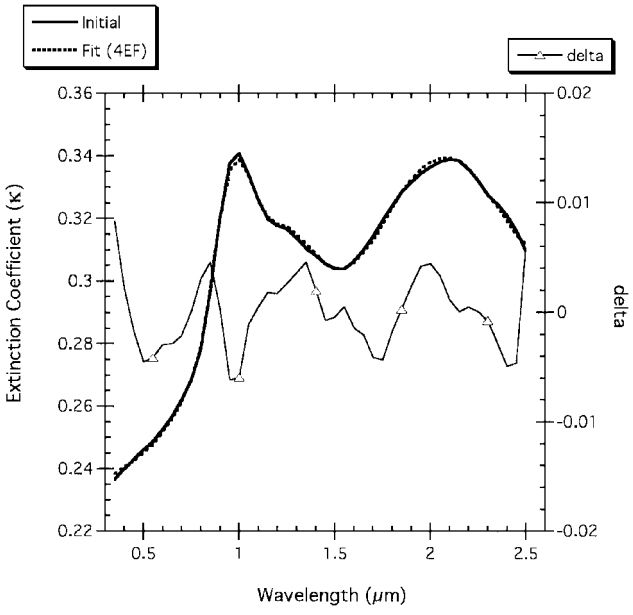

FIG. 7. An example of the actual $\kappa(\lambda)$ spectrum for the 10–20 size separate of 15071 compared to the spectrum derived from the first four eigenfunctions. The error (delta) is typically less than 1/2%.

Eigenfunctions and eigenvalues for the whole set of mare soil spectra were derived, and values for the first four are shown in Fig. 6. The first eigenfunction captures albedo variations and much of the continuum slope toward longer wavelengths. The second, third, and fourth capture major and minor variations of superimposed absorptions and continuum slope. These four eigenfunctions can be used to described any $\kappa(\lambda)$ spectrum with a relative accuracy of better than 1%. An example for the 10–20 μm fraction of 15071 is shown in Fig. 7.

The results for this PCA analysis of lunar mare soils is similar to an earlier detailed analysis by Jaumann (1991), who used a less well-controlled group of lunar sample spectra. Even though there are significant differences in the details of implementation, it is reassuring that the shape of the derived eigenfunctions for the two independent analyses are quite similar (Fig. 6 here and Figs. 3 and 4 from Jaumann, 1991).

5. PCA APPLICATIONS: LINKS BETWEEN SPECTRA AND COMPOSITION

With this compact set of independent variables for each type of data, we derive functions to link composition and spectroscopy.

We then evaluate the accuracy of predicting composition using spectrally derived parameters.

5.1. Formulation

Consider N number of spectra $\kappa_i(\lambda)$, measured at the discrete set of wavelengths λ, and associated values of K additional compositional parameters $p_{k,i}$ for each spectrum. To establish the connection between $p_{k,i}$ and the spectral properties given by spectrum $\kappa_i(\lambda)$, we need to find some unknown function $P_i = P(\kappa_i(\lambda))$ for each parameter. As demonstrated in the above principal component analysis, each spectrum can be efficiently described by a small number of derived eigenfunctions and a series of coefficients. For this analysis we assume that a linear relationship exists between the compositional parameters to be calculated $P_{i,k}$ and the set of PCA coefficients $a_{i,q}$ derived for each spectrum of the set. The general relationship between the two can be expressed in the form

$$P_{k,i} = P_{0,k} + \sum_{q=1}^{Q} w_{q,k} a_{i,q}, \tag{7}$$

where $w_{q,k}$ are weight values which are the same for all spectra for a given parameter. The objective is to find these weight functions.

Of course, the relationship expressed in Eq. (7) is not exact, and there exists some difference between the measured p_i and calculated P_i values for each parameter k:

$$\delta_i = P_i - p_i. \tag{8}$$

We can choose w_q such that the sum of all squares of the differences will be minimal:

$$S = \sum_i \delta_i^2 = \min. \tag{9}$$

This is the classical minimal least-squares method of solution, leading to a minimization of RMS error of calculated P_i. The condition of the minimum of S is

$$\begin{cases} \dfrac{\partial S}{\partial P_0} = 0, \\ \dfrac{\partial S}{\partial w_q} = 0, \quad 1 \le q \le Q. \end{cases} \tag{10}$$

For each parameter, this provides a system of linear equations, which can be solved since $N \ge Q + 1$. The weight coefficients $w_{q,k}$, for each kth chemical and mineralogical parameter, were then calculated. These are listed in Tables VII and VIII for the major compositional parameters measured for the mare soils studied.

To evaluate how well this formulation describes (and predicts) compositional parameters linear regression equations were obtained for the spectral estimations of the chemical and mineralogical parameters using the weight coefficients $w_{q,k}$. Any chemical or mineralogical parameter can be expressed as follows:

$$P_{k,i} = P_{0,k} + s_k \cdot \sum_{q=1}^{4} \frac{w_{q,k} a_{i,q}}{\beta_q}. \tag{11}$$

The weight coefficients w_q and regression coefficients $P_{0,k}$ and s_k are also listed in Tables VII and VIII, along with correlation coefficients and RMS errors. A linear relation between parameters was assumed. For I_s/FeO, however, we found that a logarithmic representation of corresponding parameters improved the results significantly and we have therefore used a logarithmic representation only for I_s/FeO in these analyses.

If the soil data set involved in this analysis is assumed to be representative, then this empirical approach can be used in a predictive sense by using a measured spectrum to estimate the composition of a soil. The steps to predict composition from a spectrum would include the following:

- Transform the bidirectional spectrum into an extinction coefficient spectrum $[\kappa(\lambda)]$.
- Model the $\kappa(\lambda)$ spectrum with the principal eigenfunctions (φ_q) (e.g., Fig. 6; $q = 4$) and average spectrum $\bar{\kappa}(\lambda)$ of the data set to derive the loading coefficients a_q for each eigenfunction for the spectrum.

TABLE VII

Weight Coefficients w_q, Regression Coefficients s, P_0, RMS Error σ^*, and Correlation Coefficients c^* for Spectral Estimation of Chemical Parameters

k		$w_{1,k}$	$w_{2,k}$	$w_{3,k}$	$w_{4,k}$	s_k	$P_{0,k}$	σ_k (%)	c
1	SiO_2	−0.284	0.199	0.500	0.571	14.1	43.6	1.55	0.83
2	TiO_2	0.266	−0.293	−0.404	0.657	14.7	6.01	1.47	0.87
3	Al_2O_3	0.337	0.811	0.193	−0.148	9.79	13.0	0.80	0.91
4	MgO	−0.238	−0.195	−0.259	0.714	5.33	9.92	0.61	0.82
5	FeO	−0.398	−0.764	−0.227	0.102	10.1	15.4	0.89	0.90
6	$\log(I_s)$	0.780	0.485	0.066	0.170	1.47	2.91	0.10	0.94

* Between measured and estimated values.

TABLE VIII

Weight Coefficients w_q, Regression Coefficients s, P_0, RMS Error σ^*, and Correlation Coefficients c^* for Spectral Estimation of Mineralogical Parameters

k		$w_{1,k}$	$w_{2,k}$	$w_{3,k}$	$w_{4,k}$	s_k	$P_{0,k}$	σ_k (%)	c
1	Ilmenite	0.154	−0.181	−0.376	−0.598	17.1	5.51	2.29	0.74
2	Plagioclase	0.232	0.242	−0.0545	−0.194	9.00	16.31	1.66	0.39
3	Pyroxene	−0.386	−0.742	0.297	0.335	31.5	14.5	2.09	0.94
4	Olivine	−0.462	−0.311	−0.332	0.0726	5.51	2.99	0.83	0.65
5	AggGlass	0.472	0.609	0.181	0.107	49.8	41.4	4.99	0.80
6	VolGlass	−0.240	0.0600	−0.600	−0.426	26.1	6.76	3.29	0.78

* Between measured and estimated values.

- Use this information in Eq. (11) with the appropriate weight and regression coefficient values (e.g., Tables VII and VIII) and corresponding β_q to derive the composition for the material represented by the spectrum.

5.2. Results

Comparisons of the measured chemical and mineral parameters to those derived from the spectral coefficients are shown in Figs. 8 and 9. Full LSCC data presented in Pieters *et al*. (2000b) and Taylor *et al*. (2001b) can be found at http://www.planetary.brown.edu/pds/database.html and http://web.utk.edu/~pgi/data.html. For ease of comparison, high-Ti soils (Apollos 11 and 17) are distinguished from low-Ti soils (Apollos 12 and 15) in these figures. The diagonal line represents a perfect prediction. As a test of the validity of the method, only data for the size separates (45–20, 10–20, and <10 μm) were used in derivation of

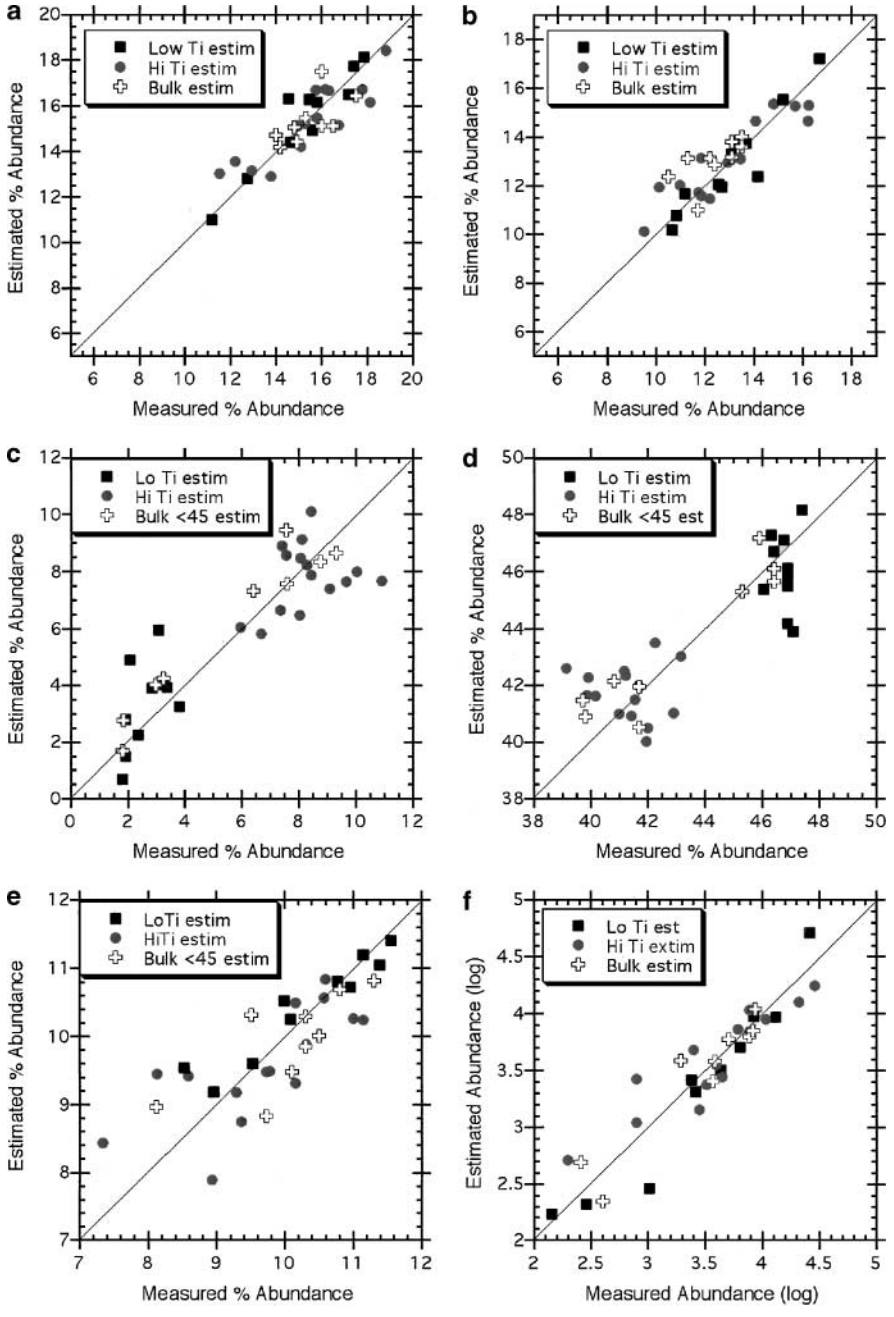

FIG. 8. Comparison of measured values of composition with values estimated from integrated spectral analyses: (a) FeO, (b) Al_2O_3, (c) TiO_2, (d) SiO_2, (e) MgO, (f) log I_s/FeO.

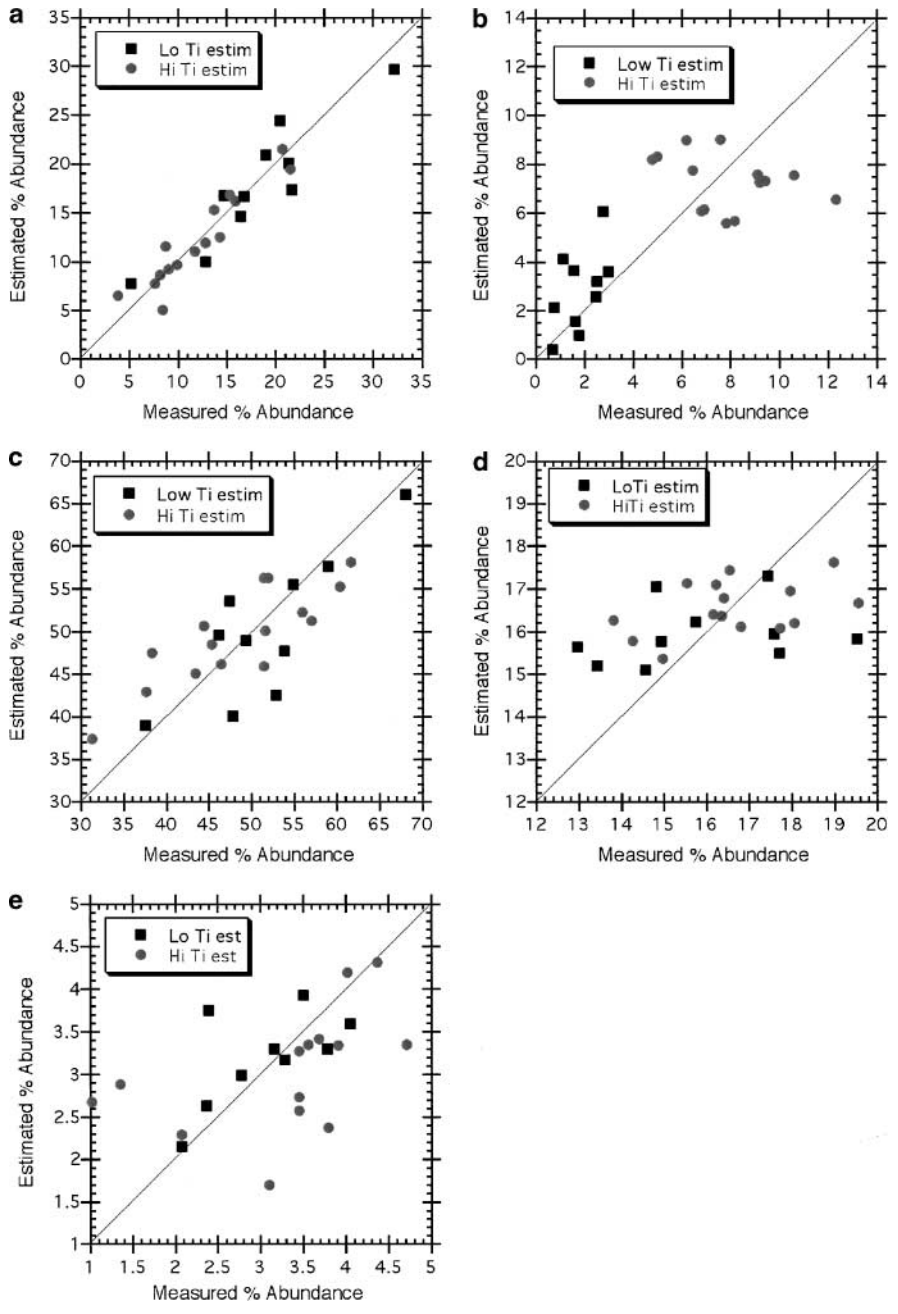

FIG. 9. Comparison of measured values of mineral abundance with values estimated from integrated spectral analyses: (a) pyroxene, (b) ilmenite, (c) agglutinates, (d) plagioclase, (e) olivine.

the weighting functions for the chemical data. Data for the bulk <45-μm sample were not included, but instead their composition is predicted from their spectra in the manner outlined above. The estimations shown in Fig. 8 not only show the accuracy achieved for the size separates of these nine soils but also illustrate how the method works equally well for independently predicting the composition of the bulk soil. Furthermore, by using the full range of spectral properties in the PCA analysis, the correlation between predicted and measured composition (Tables VII and VIII) is significantly improved over the predictions from simple correlation with spectral parameters (e.g., Fig. 4).

One of the notable results of this analysis is the relatively good empirical prediction of FeO abundance (RMS error $<1\%$) for these mare soils (Fig. 8.), even though they are all relatively iron-rich. This association with FeO is not surprising since the effect of ferrous iron on optical properties is well documented. What is less clear at this stage is the specific species that carry

the signature. Although Al_2O_3 has no direct effect on optical properties, its strong anticorrelation with FeO also produces a relatively high predictive capability from spectra.

Similarly, the high accuracy in predicting the abundance of pyroxene (Fig. 9) should be expected since iron-bearing pyroxene is one of the most optically active components of lunar soil. What is particularly encouraging is that the bulk abundance is accurately modeled in spite of the range in soil maturity of these samples (see Taylor *et al*. 2000, 2001a,b).

Given the high accuracy for Al_2O_3, it might seem odd that the abundance of plagioclase is so poorly modeled with these data. This relation is an obvious result, however, when one acknowledges processes that occur during soil evolution. The plagioclase that is gradually concentrated in the finest fraction is also readily melted and incorporated into agglutinitic glass. Plagioclase as a mineral is lost, but its chemical signature remains (Taylor *et al*. 2000, 2001b).

The accuracy for predicting TiO_2 or ilmenite is disappointing (RMS error 1.5 and 2.3% respectively). High- and low-Ti mare soils are readily distinguished, but these statistics suggest that making subclass distinctions of mare soils based on spectral predictions of TiO_2 would be risky at present.

6. FUTURE DIRECTIONS

We are encouraged by the initial results of this purely statistical (empirical) analysis of relationships between the visible to near-infrared spectral properties and compositional data for mare soils. There are very definite relations which can be quantified, some of which are stronger than others. The origin of most, but not all, relations are readily identified and are linked to physical properties of minerals (e.g., Burns 1993) and soil formation processes (Pieters *et al*. 2000a, Taylor *et al*. 2001b).

Because of the limited range of data used in this analysis (only mare soils), however, it would be premature to recommend these results be used for estimating composition from spectral analysis. Nevertheless, the existence of clear relations between optical properties of lunar soils and composition is abundantly evident. Several additional directions stimulated by these analyses merit further study to bring this empirical approach to a level that can be used reliably for compositional predictions.

First, expansion of the input data to include a broader range of soil compositions is desperately needed. Specifically, a comparable suite of carefully selected highland soils would extend the foundation to include the most abundant soil type on the Moon: soils that are high Al, low Fe, and low Ti. Use of empirical methods for predicting composition is only as good as the input data. Without a wide range of known compositions bounding the input data, little confidence can be placed in using estimations of composition for unknown targets.

Second, from the practical standpoint, it would be quite useful to reconfigure these (and future analyses) with the limited spectral range of data currently available for the Moon (Clementine multispectral images). The data presented here rely on precise spectral data over the broad range of reflected radiation (0.3 to 2.6 μm) and are essential for a complete analysis of the possibilities. However, missions have not necessarily provided the "optimum" spectral range and coverage for remote global data. It would be most instructive and useful to compare results using the five channels of the Clementine UVVIS to these more complete analyses. Although the five-channel results are likely to be less accurate than these produced with full spectra, the Clementine data provide the backdrop for much of lunar remote sensing data available for the next several years.

A principal aspect that has not been thoroughly explored is the ability to reliably distinguish among different types of mafic minerals. As can be seen in Table II, analyses of mineral abundance for the soil suite has been carried out to differentiate among different compositions of pyroxene. For the statistical study presented here, we have grouped them all together. One of the most promising methods for quantitatively assessing the relative proportion of different types of pyroxene present is tied to the deconvolution of the ferrous absorption band into individual components (Sunshine *et al*. 1990). This has worked quite well for the initial suite of mare soils (Noble *et al*. 2000) and will be an essential direction to pursue with the more extensive suite of data.

ACKNOWLEDGMENTS

Partial support for this work from NASA Solar System Exploration is gratefully acknowledged. The authors appreciate the thoughtful reviews by R. Jaumann and an anonymous reviewer.

REFERENCES

Adams, J. B. 1974. Visible and near-infrared diffuse reflectance spectra of pyroxenes as applied to remote sensing of solid objects in the Solar System. *J. Geophys. Res.* **79**, 4829–4836.

Blewett, D. T., P. G. Lucey, B. R. Hawke, and B. L. Jolliff 1997. Clementine images of the lunar sample-return stations: Refinement of FeO and TiO_2 mapping techniques. *J. Geophys. Res.* **102**, 16,319–16,325.

Burns, R. G. 1993. *Mineralogical Application of Crystal Field Theory.* Cambridge Univ. Press, Cambridge, UK.

Charette, M. P., T. B. McCord, C. M. Pieters, and J. G. Adams 1974. Application of remote spectral reflectance measurements to lunar geology classification and determination of titanium contents of lunar soils. *J. Geophys. Res.* **79**, 1605–1613.

Fischer, E. M. 1995. *Quantitative Compositional Analysis of the Lunar Surface from Reflectance Spectroscopy: Iron, Aluminum and a Model for Removing the Optical Effects of Space Weathering*. Ph.D. dissertation, Brown University, Providence, RI.

Fischer, E. M., and C. M. Pieters 1995. Lunar surface aluminum and iron concentration from Galileo solid state imaging data, and the mixing of mare and highland materials. *J. Geophys. Res.* **100**, 23,279–23,290.

Hapke, B. 1981. Bidirectional reflectance spectroscopy 1: Theory. *J. Geophys. Res.* **86**, 3039–3054.

Hapke, B. 1993. *Theory of Reflectance and Emittance Spectroscopy.* Cambridge Univ. Press, New York.

Heiken, G. H., D. T. Vaniman, and B. M. French, Eds. 1991. *Lunar Sourcebook, A User's Guide to the Moon*. Cambridge Univ. Press, Cambridge.

Hiesinger, H., R. Jaumann, G. Neukum, and J. W. Head III 2001. Ages of mare basalts on the lunar nearside. *J. Geophys. Res.* **105**, (E12), 29239–29275.

Hiroi, T., and C. M. Pieters 1992. Effects of grain size and shape in modeling reflectance spectra of mineral mixtures. *Proc. Lunar Planet. Sci.* **22**, 313–325.

Hiroi, T., and C. M. Pieters 1994. Estimation of grain sizes and mixing ratios of fine powder mixtures of common geologic minerals. *J. Geophys. Res.* **99**, 10,867–10,879.

Jaumann, R. 1991. Spectral-chemical analysis of lunar surface materials. *J. Geophys. Res.* **96**, 22,793–22,807.

Johnson, J., T. Swindle, and P. G. Lucey 1999. Estimated solar wind-implanted helium-3 distribution on the Moon. *Geophys. Res. Lett.* **26**, 385–388.

Johnson, J. R., and R. B. Singer 1991. A reevaluation of spectral ratios for lunar mare TiO_2 mapping. *Geophys. Res. Lett.* **18**, 2153–2156.

Johnson, P. E., M. O. Smith, and J. B. Adams 1985. Quantitative analysis of planetary reflectance spectra with principal components analysis. Proc. Lunar & Planet. Sci. Conf. 15th, Part 2, *J. Geophys. Res.* **90**, C805–C810.

Keller, L. P., S. Wentworth, D. S. McKay, L. A. Taylor, C. M. Pieters, and R. V. Morris 2000. Space weathering in the fine size fractions of lunar soils mare/highland differences. *Lunar Planet. Sci.* **31**, 1655 (abstract).

Lucey, P. G., G. Taylor, and E. Malaret 1995. Abundance and distribution of iron on the Moon. *Science* **268**, 1150–1153.

Lucey, P. G., G. J. Taylor, B. R. Hawke, and P. D. Spudis 1998. FeO and TiO_2 concentrations in the South Pole–Aitken basin: Implications for mantle composition and basin formation. *J. Geophys. Res.* **103**, 3701–3708.

Lucey, P. G., D. T. Blewett, and B. L. Joliff 2000. Lunar iron and titanium abundance algorithms based on final processing of Clementine untraviolet–visible images. *J. Geophys. Res.* **105**, 20,297–20,306.

Morris, R. V. 1976. Surface exposure indices of lunar rocks: A comparative FMR study. *Proc. Lunar Planet. Sci.* **7**, 315–335.

Morris, R. V. 1978. The surface exposure (maturity) of lunar soils: Some concepts and Is/FeO compilation. *Proc. Lunar Planet. Sci.* **9**, 2287–2297.

Noble, S. K., C. M. Pieters, T. Hiroi, L. A. Taylor, R. V. Morris, L. P. Keller, D. S. McKay, and S. Wentworth 2000. Initial results of MGM analysis on Apollo 17 Soil Suite. *Lunar Planet. Sci.* **31**, 1880 (abstract).

Noble, S. K., C. M. Pieters, L. A. Taylor, R. V. Morris, C. C. Allen, D. S. McKay, and L. P. Keller 2001. The optical properties of the finest fraction of lunar soils: Implications for space weathering environments. *Meteorit. Planet. Sci.* **36**, 31–42.

Pieters, C. M. 1978. Mare basalt types on the front side of the Moon: A summary of spectral reflectance data. *Proc. Lunar Planet. Sci.* **9**, 2825–2849.

Pieters, C. M. 1993. Compositional diversity and stratigraphy of the lunar crust derived from reflectance spectroscopy. In *Remote Geochemical Analysis: Elemental and Mineralogical Composition* (C. M. Pieters and P. A. J. Englert, Eds.), pp. 309–339. Cambridge Univ. Press, Cambridge, UK.

Pieters, C. M., E. M. Fischer, O. Rode, and A. Basu 1993a. Optical effects of space weathering: The role of the finest fraction. *J. Geophys. Res.* **98**, 20,817–20,824.

Pieters, C. M, and 11 colleagues 1993b. Crustal diversity of the Moon: Compositional analyses of Galileo solid state imaging data. *J. Geophys. Res.* **98**, 17,127–17,148.

Pieters, C. M., L. A. Taylor, S. K. Noble, L. P. Keller, B. Hapke, R. V. Morris, C. C. Allen, D. S. McKay, and S. Wentworth 2000a. Space weathering on airless bodies: Resolving a mystery with lunar samples. *Meteorit. Planet. Sci.* **35**, 1101–1107.

Pieters, C. M., L. A. Taylor, D. S. McKay, S. Wentworth, R. V. Morris, and L. P. Keller 2000b. Spectral characterization of lunar mare soils. *Lunar Planet. Sci.* **31**, 1865 (abstract).

Shkuratov, Y. G., V. G. Kaydash, and N. V. Opanasenko 1999a. Iron and titanium abundance and maturity degree distribution on lunar nearside. *Icarus* **137**, 222–234.

Shkuratov, Y. G., L. V. Starukhina, V. G. Kaydash, and N. V. Bondarenko 1999b. Distribution of ^{3}He abundance over the lunar nearside. *Sol. Syst. Res.* **33**, 409–420.

Shkuratov, Y. G., L. V. Starukhina, H. Hoffman, and G. Arnold 1999c. A model of spectral albedo of particulate surfaces: Implications for optical properties of the Moon. *Icarus* **137**, 234–246.

Sunshine, J. M., C. M. Pieters, and S. F. Pratt 1990. Deconvolution of mineral absorption bands: An improved approach. *J. Geophys. Res.* **95**, 6955–6966.

Taylor, L. A., C. M. Pieters, R. V. Morris, L. P. Keller, D. S. McKay, A. Patchen, and S. Wentworth 2000. Space weathering of lunar mare soils: New understanding of the effects on reflectance spectroscopy. *Space 2000, Proc. Am. Soc. Civil Eng.* pp. 703–711.

Taylor, L. A., C. M. Pieters, R. V. Morris, L. P. Keller, D. S. McKay, A. Patchen, and S. Wentworth 2001a. The effects of space weathering on Apollo 17 mare soils: Petrographic and chemical characterization. *Meteorit. Planet. Sci.* **36**, 285–300.

Taylor, L. A., C. M. Pieters, R. V. Morris, L. P. Keller, and D. S. McKay 2001b. Lunar mare soils: Space weathering and the major effects of surface-correlated nanophase Fe. *J. Geophys. Res.* **106**, E11, 27,985–28,000.